ACS OMEGA

http://pubs.acs.org/journal/acsodf

Article

Highly Sensitive Molecularly Imprinted Polymer-Based Electrochemical Sensors Enhanced by Gold Nanoparticles for Norfloxacin Detection in Aquaculture Water

Oanh Thi Vu, Quoc Hao Nguyen, Tin Nguy Phan, Thanh ThuyThi Luong, Kasper Eersels, Patrick Wagner, and Lien Thi Ngoc Truong*

Cite This: *ACS Omega* 2023, 8, 2887−2896

Read Online

ACCESS | Metrics & More | Article Recommendations

ABSTRACT: The overuse of antibiotics in aquaculture and pharmaceuticals and their subsequent leaking into the environment have been demonstrated to be a potential route for creating antibiotic resistance in bacteria. In order to assess the impact of this problem and take regulatory measures, it is necessary to develop tools that allow for the detection of antibiotics in environmental samples in a routine, low-cost manner. In this study, we integrated gold nanoparticles (AuNPs) into a molecularly imprinted polymer (MIP) membrane to fabricate a new sensor for the detection of norfloxacin in pharmaceuticals and aquaculture samples. The receptor layers were characterized by scanning electron microscopy, electrochemical impedance spectroscopy, and Raman spectroscopy. The results of these studies demonstrate that the addition of AuNPs to the polymer network enhanced the sensor sensitivity by at least a factor of two. The MIP−AuNPs sensor has a low detection limit (0.15 ng/mL, $S/N = 3$) with a wide linear range and very high sensitivity. The selectivity of the fabricated sensor was measured in the sample containing other antibiotics (like chloramphenicol, ciprofloxacin, and levofloxacin). Rapid and precise norfloxacin detection in pharmaceutical compounds and fishpond water samples indicates that the fabricated sensor has the potential to be used for routine screening of aquacultures and pharmaceutical processes.

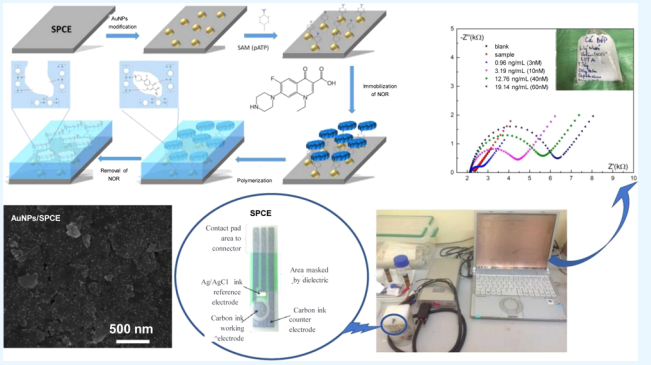

1. INTRODUCTION

For many years, antibiotics have been widely used for the prevention and treatment of human and animal diseases.[1] Norfloxacin (NOR), a second-generation fluoroquinolone type antibacterial, is a common antibiotic that has been abused in medicine and animal husbandry because of its large-spectrum antimicrobial activity against various pathogenic Gram-negative and Gram-positive bacteria such as gentamicin-resistant Pseudomonas.[2] NOR has been usually used for the treatment of some infections in both humans and animals for many years.[3] However, it may lead to some side effects including headache, depression, dizziness, nausea, and vomiting. Although it is no longer available in the US since 2014,[4] there are a lot of reports of the residue of NOR in medicine in the rest of the world.[5,6] Of importance, NOR is difficult to degrade in the environment. Meanwhile, only a low NOR concentration can upgrade the residence of bacteria.[6]

Up to now, many analytical techniques have been developed for the measurement of NOR concentration, namely, high-performance liquid chromatography (HPLC),[7] coupled gas chromatography−mass spectrometry,[8] ion mobility spectroscopy,[9] surface-enhanced Raman scattering,[10] and TeraHertz spectroscopy.[11] Although most techniques can perform excellent stability with accuracy, they require costly equipment and a complex sample preparation process and need to be used in a lab environment. These techniques are therefore not suitable to be deployed on a large scale in the field to screen samples and take preventive and regulatory measures. Thus, it is necessary to develop new techniques that allow for highly sensitive, rapid, low-cost, and efficient detection of NOR.[12,13]

The key to creating a good biosensor is coupling a suitable read-out methodology to a specific receptor layer that is able to detect the target with limited cross-selectivity observed. Molecularly imprinted polymers (MIPs) are a class of synthetic receptors that have been demonstrated to be extremely useful for biosensor applications due to their inherent selectivity.[14]

Received: July 13, 2022
Accepted: December 26, 2022
Published: January 9, 2023

MIPs are typically made by creating a cross-linked polymer network around the analyte of interest, often via free radical polymerization. After removing the analyte or template, nanocavities will be introduced in the bulk of the polymer or the surface of a polymer film that is complementary in size and shape to the template but also have a complementary distribution of functional groups due to molecular interaction during the polymerization process.[15,16] The binding sites created in these cavities result in an affinity and selectivity of the MIPs for their target that is similar to that of natural receptors such as antibodies or enzymes. The approach has been used extensively to create receptors for MIP-based sensing for a wide array of targets ranging from small chemical substances to large biological entities.[17,18] Despite the fact that bioreceptors are generally still superior in terms of binding affinity and selectivity, MIPs have several advantages including their thermal and chemical stability, nearly unlimited shelf-life, and their ethical, low-cost, and straightforward synthesis process.[19,20]

MIPs have been used extensively as synthetic receptors in biosensor platforms for antibiotics by combining them with thermal, optical, colorimetric, and gravimetrical transducer principles.[21,22] However, the combination of MIPs with electrochemical readout techniques has proven to be particularly interesting due to the low detection limit (LoD) that can be achieved and the commercial success of electrochemical biosensors.[23] In this work, we, therefore, developed a MIP-based electrochemical sensor for the detection of NOR in real samples. To boost the sensitivity of the sensor, we deposited the MIP layer onto a screen-printed carbon ink electrode (SPCE) and doped the MIP layer by introducing gold nanoparticles (AuNPs), in which AuNPs were integrated into the MIP layer by two methods. The two methods are simple, inexpensive, and easy to conduct, which may lead to the trend in the development of biosensors based on the MIP technique. The fabrication process could be monitored in a stepwise fashion using electrochemical impedance spectroscopy (EIS) as the morphology changes at each step, thereby altering the double-layer capacitance and charge transfer resistance at the interface. For electrochemical sensors, especially EIS sensor, the conductivity of the electrode has a substantial impact on the sensor's sensitivity. Furthermore, the self-assembled monolayer (SAM) film formed from *p*-ATP molecules is considered to be more stable and conductive than others like *o*-ATP and *m*-ATP. To create high conductivity MIP membranes, the 4-aminothiophenol (*p*-ATP) monomer was chosen. In addition, thanks to the low oxidation of *p*-ATP, electropolymerization can be carried out at a low voltage.[24] As a result, electrochemical procedures have a negligible influence on biomolecules. Furthermore, the amine functional groups of poly(aminophenol) were expected to make a specific bond with the target. The performance of the sensor in rebinding the template in complex samples was also assessed using EIS, illustrating the positive effect of doping the MIP layer with AuNPs. The resulting sensor was demonstrated to have a LoD of 0.15 ng/mL and a wide linear range that proves the platform could potentially be used for the rapid and on-site screening of environmental and aquaculture samples for the presence of bacteria.

2. EXPERIMENTAL SECTION

2.1. Chemicals and Apparatus. In this work, all chemicals and reagents were highly purified (>99%) and utilized without any purification. NOR, mono *para*-aminothiolphenol (*p*-ATP), and tetrachloroauric(III) acid trihydrate ($HAuCl_4{\cdot}3H_2O$) were purchased from Sigma-Aldrich, Germany. Deionized (DI) water had a resistance of more than 18 MΩ•cm. Phosphate-buffered saline (PBS) with a concentration of 100 mM was prepared from potassium phosphates (K_2HPO_4 and KH_2PO_4) and sodium chloride (NaCl) in DI. Potassium hexacyanoferrate(II) ($K_4Fe(CN)_6$) and potassium hexacyanoferrate(III) ($K_3Fe(CN)_6$) with concentrations of 5 mM were prepared in 0.1 M KCl solution for EIS measurements. NOR was dissolved in 1% acid acetic (CH_3COOH) to obtain different concentrations. Ethanol and distilled water were used for washing electrodes.

The electrodes used for sensor fabrication are screen-printed carbon electrodes (SPCEs) from BioDevice Technology, Japan. The structure of this electrode chip consists of three electrodes, including a carbon-ink working electrode with an area of 2.64 mm^2, a counter electrode (carbon ink), and a reference electrode (Ag/AgCl ink), integrated on a plastic substrate. All electrochemical measurements were conducted using a potentiostat (Ivium Technologies, Netherlands).

In addition, scanning electron microscopy (SEM) (NANO-SEM450, Netherlands) and Raman spectroscopy (Renishaw inVia Raman, wavelength of 633 nm) were used to analyze the surface characteristics of the sensors.

2.2. Sensor Fabrication. *2.2.1. Preparation of AuNPs/SPCE.* The working electrode of the SPCE chip was modified by AuNPs via the cyclic voltammetry (CV) technique.[25,26] In particular, 35 μL of PBS solution (pH 7.4) containing 100 μM $HAuCl_4$ was dropped on the surface of the electrode. Then, the potential range from −0.6 to 0.5 V versus Ag/AgCl was applied for 20 cycles to fabricate AuNPs on the electrode surface. Next, the electrode was continuously scanned in the solution of 1 M H_2SO_4 with a potential range from −0.2 to 1.4 V versus Ag/AgCl for five cycles to clean the electrode and remove the gold oxide layer. Then, the obtained AuNPs/SPCE chip was washed with distilled water twice and dried with N_2.

2.2.2. Preparation of SAM (p-ATP)/AuNPs/SPCE. The AuNP-coated SPCEs were immersed in a 50 mM *p*-ATP monomer solution for 15 h at room temperature in a dark room. During the process, a SAM of *p*-ATP molecules could be formed on the electrode surface via the binding of the thiol −SH group of *p*-ATP with AuNPs. As a result, the electrode was coated with a *p*-ATP SAM with the $-NH_2$ groups facing outward to the solution [SAM (*p*-ATP)/AuNPs/SPCE]. The $-NH_2$ group, with high biocompatibility, easily forms covalent bonds with −COOH and acts as an oxidizing target to create the main chain and a crosslinker in the polymerization process. Furthermore, the SAM of the *p*-ATP molecule shows better stability and electrical conductivity than other isomers of aniline like *o*-ATP and *m*-ATP.

2.2.3. Attaching NOR Molecules to the SAM (p-ATP)/AuNPs/SPCE. To immobilize NOR molecules onto the SAM, 35 μL of PBS solution containing 1% NOR and 1% acetic acid was dropped on the electrode surface. Then, a static potential of −0.6 V versus Ag/AgCl was applied for 600 s. In this step, the amine functional groups of NOR molecules were protonated. As a result, the NOR molecules were drawn close to the electrode surface. Also, they were bound to the SAM by electrostatic attraction at a constant negative potential.

2.2.4. Polymerization of NOR-MIP onto AuNPs/SPCE. The solution used for polymerization consisted of 10 mM *p*-ATP

https://doi.org/10.1021/acsomega.2c04414
ACS Omega 2023, 8, 2887−2896

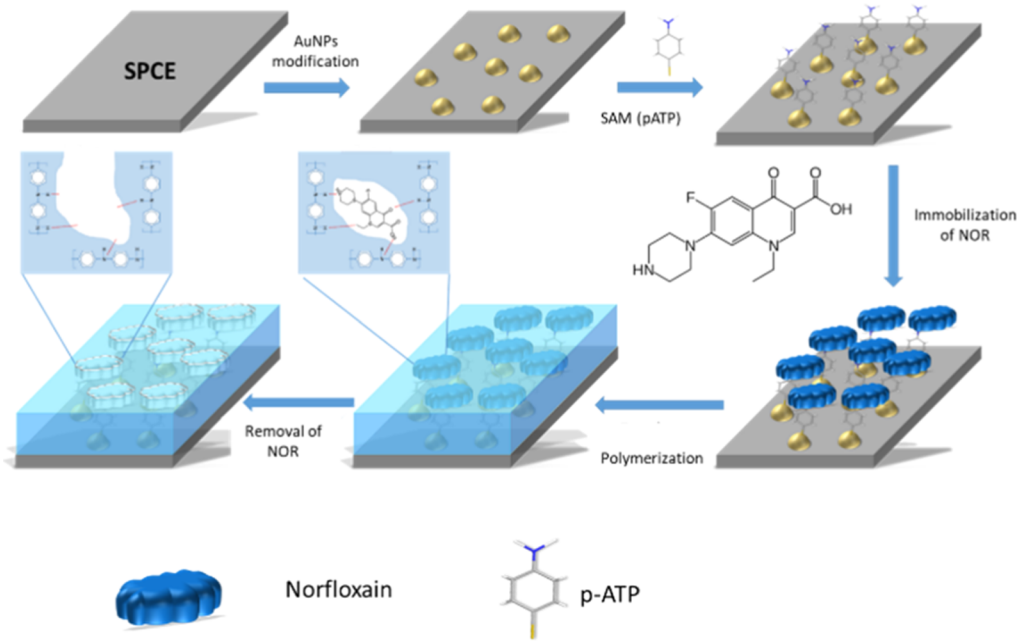

Figure 1. Scheme for the fabrication of the NOR-MIP/AuNPs/SPCE sensor. Step 1: modification of the working electrode of the SPCE chip by AuNPs via the CV technique (AuNPs/SPCE); step 2: modification of AuNPs/SPCE by a SAM of *p*-ATP molecules [SAM (*p*-ATP)/AuNPs/SPCE]; step 3: attaching NOR molecules to the SAM (*p*-ATP)/AuNPs/SPCE; step 4: polymerization of NOR-MIP onto AuNPs/SPCE; and step 5: NOR extraction to create NOR-MIP/AuNPs/SPCE sensor.

monomer and 2.5 mM NOR in 100 mM PBS buffer. 35 μL of this solution was dropped onto the prepared electrode and the CV technique with an applied potential range of from −0.2 to +0.6 V versus Ag/AgCl with a scan rate of 50 mV/s was carried out in 20 cycles. The polymer film was formed through the conjugated polymer bonding of the electron pair of the nitrogen atom of the *p*-ATP molecule, forming a poly-(aminothiophenol) chain with an alternating structure between a phenyl ring and a nitrogen-containing functional group. In an environment with a pH of 6.6, the N atoms were protonated to a certain extent, creating charge carriers that form in the polymer matrix, making the polymer-MIP film conductive. During the polymerization process, NOR molecules and the *p*-ATP molecules of the polymer network formed specific binding sites through non-covalent interaction. The amine group of the polymer could react with the hydrogen and oxygen groups in the template through hydrogen bonding. Additionally, the −N and $-CH_3$ group of NOR could interact with the −H and $-NH_2$ groups of *p*-ATP, respectively. To extract the template, the electrode was then washed with ethanol and twice with distilled water and dried with N_2.

Furthermore, AuNPs were doped into the polymer network to enhance the signal of the sensor by two different approaches. In the first method, a large amount of $HAuCl_4$ was added to the polymer solution. At a reduction potential of −0.45 V versus Ag/AgCl, Au was reduced and immediately embedded in the polymer network during polymerization. Therefore, we selected the potential range for polymerization from −0.5 to 0.6 V versus Ag/AgCl. For the second methodology, a quantity of 10 nm gold particles was bound to the *p*-ATP monomer in the polymer solution and then polymerization was carried out with the voltage swept from −0.2 to 0.6 V versus Ag/AgCl.

2.2.5. NOR Extraction. To remove the NOR molecule from the polymer-MIP, we dripped 35 μL of 1 M HCl onto the electrode obtained in the previous step and applied a static potential of 0.6 V versus Ag/AgCl for 600 s. The process of extraction of NOR molecules from the polymer network can be explained based on the electrostatic interaction. When a constant positive potential was applied to the electrode in a strongly acidic medium, the −OH groups and the $-NH_2$ groups were protonated, leading to weak bonds that were easily broken. The utilization of positive voltage boosted the breaking of the bond between the NOR molecule and the polymer network faster. After the extraction step, the artificial bio-receivers of the NOR molecule were created by MIP technology (NOR-MIP). The electrode was then carefully rinsed with ethanol and twice with distilled water and dried with a stream of N_2. Next, the electrode was immersed in a 100 mM PBS solution (pH 6.8) to stabilize it. The scheme for the fabrication of the NOR-MIP/AuNPs/SPCE sensor is shown in Figure 1.

A non-imprinted polymer (NIP) sensor (NIP/AuNPs/SPCE) was fabricated using the same process as the NOR-MIP/AuNPs/SPCE without introducing the template during polymerization.

3. RESULTS AND DISCUSSION

3.1. Characteristics of the NOR-MIP/Au/NPs/SPCE. In this part, we examined the characteristics of the sensor after each modification step to confirm the successful fabrication of the sensor. The most important feature of the sensor is the formation of a polymer layer with specific imprinters. Figure 2a represents the CV curve during the polymerization procedure. The results show that the current response decreases after each scan and there is a clear oxidation peak at +0.24 V versus Ag/AgCl due to the polymerization of the *p*-ATP monomer.[27] In the first cycle, there was a large number of monomers reacting, leading to the largest response current (4.9 μA). Throughout each cycle, the response current at the oxidation peak decreases (the response current at the second cycle is 3.5

https://doi.org/10.1021/acsomega.2c04414
ACS Omega 2023, 8, 2887−2896

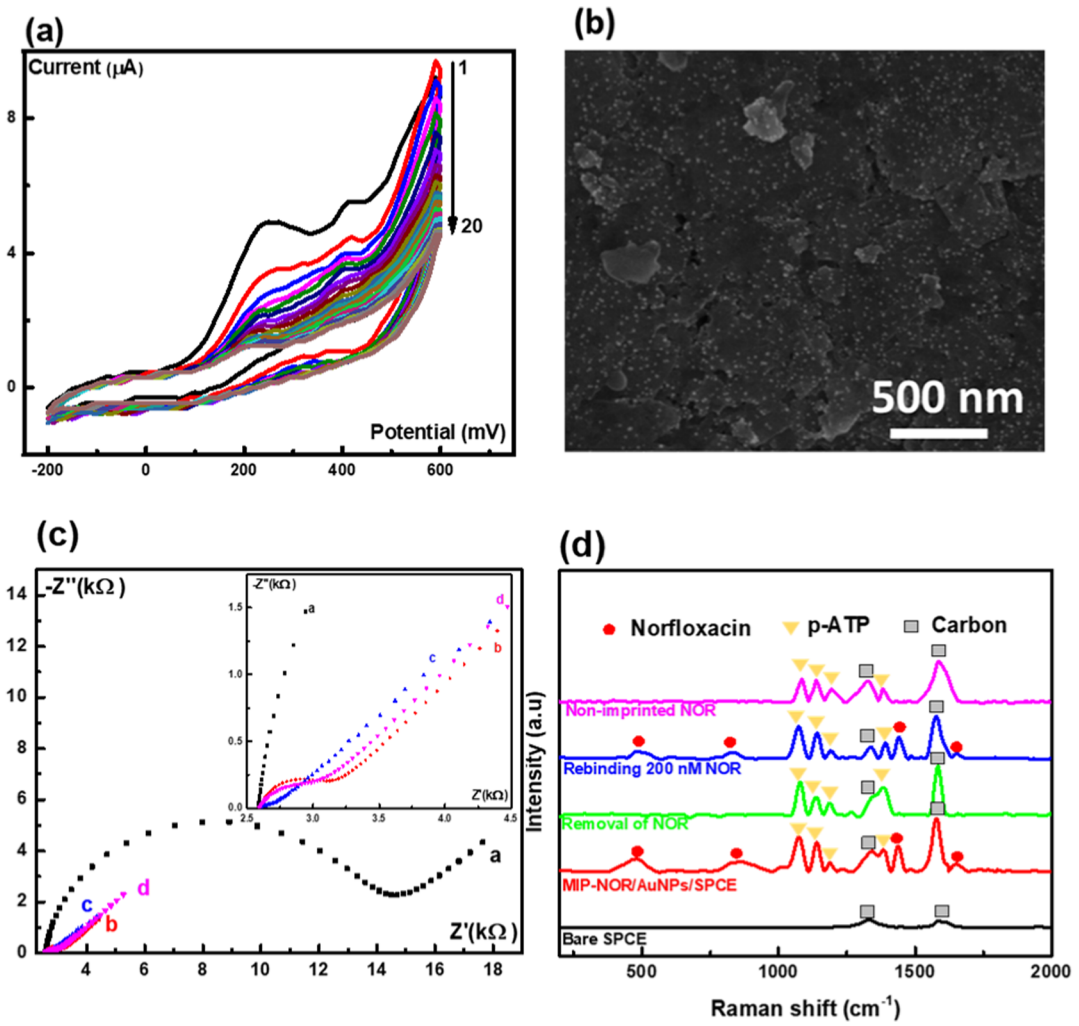

Figure 2. (a) CV plots of the modification of AuNPs on the SPCE; (b) SEM image of the AuNP-modified SPCE; (c) EIS spectrum of (a) SPCE, (b) AuNPs/SPCE, and (c,d) NOR-MIP/AuNPs/SPCE before and after removing NOR; and (d) Raman spectrum of the fabricated sensors.

μA), indicating that the amount of monomer decreases, leading to a decrease in the response current. NOR molecules were not involved in the polymerization process, and so, their structure was not affected.

Figure 2b shows the SEM images of the morphologies of the electrode after 20 scans. It can be seen that there are many small and uniform light spots on the surface of the electrode, which are AuNPs. However, these spots are quite faint because of a thin film covering the electrode. Based on a uniform SAM membrane of *p*-ATP molecules on AuNPs/SPCE, the outward $-NH_2$ groups of the SAM membrane will crosslink with each other to create a polymer network. Due to the thin layer of the MIP membrane, we can easily remove the NOR molecules from the polymer network to create specific cavities. These results confirm that a dense polymer layer can be formed on the AuNP-modified SPCE using CV.

Figure 2c shows the EIS analysis of the electrode after each modification step. The values of R_{CT} were calculated based on the equivalent Randle circuit. For the bare carbon-printed electrode, the value of R_{CT} is very high (12.0 kΩ). This value was significantly reduced to 0.8 kΩ after modification with AuNPs. This implies that the AuNP layer increases the charge transfer capacity of the electrode, thereby decreasing the charge transfer resistance. Polymerization of the *p*-ATP monomer on the AuNPs−SPCE results in a very small semicircle in the Nyquist plot, resulting from *p*-ATP's conductivity thereby further reducing the charge transfer resistance. Then, after extraction of the NOR molecules, the charge transfer resistance slightly increases again but remains at very small (0.3 kΩ). Due to the thin MIP layer, NOR molecules were removed from the membrane easily. As a result, a network of holes was formed, which caused the membrane to become uneven, thereby slightly increasing the value of the charge transfer resistance. However, the cavities allow for the diffusion of the redox probes and the transfer of charge to the electrode smoothly. When the analytes and the specific cavities were recombined together, the number of empty cavities decreased. As a result, the transport of electrons to the substrate is more difficult, leading to an increase in the R_{CT}. The difference in the charge transfer resistance (ΔR_{CT}) value before and after the NOR molecule recombined with the cavities was selected as the sensor output signal.

Figure 2d represents the Raman spectra of the fabricated sensor recorded after each modification step. First, in the Raman spectrum of a carbon-printed electrode, there are two peaks recorded at 1580 and 1337 cm^{-1}, corresponding to oscillations of the C−C bond in the carbon lattice (G-band) and defects in the carbon lattice (D-band), respectively.[28,29]

https://doi.org/10.1021/acsomega.2c04414
ACS Omega 2023, 8, 2887−2896

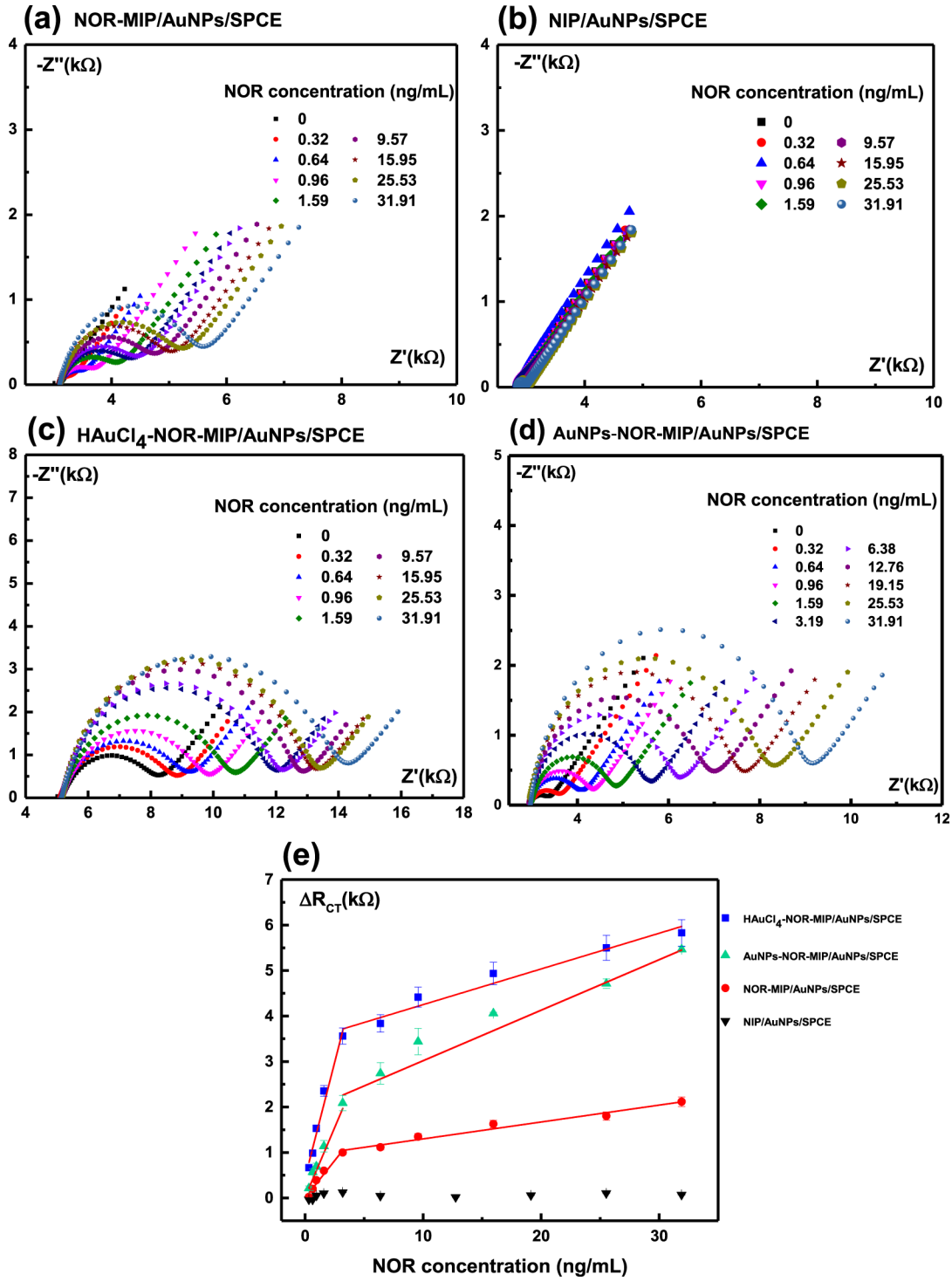

Figure 3. EIS spectrum of (a) NOR-MIP/AuNPs/SPCE, (b) NIP/AuNPs/SPCE, (c) $HAuCl_4$-NOR-MIP/AuNPs/SPCE, (d) AuNPs-NOR-MIP/AuNPs/SPCE toward different NOR concentrations; and (e) calibration plot of the independence of ΔR_{CT} on NOR concentration.

After forming a polymer membrane with NOR antibiotics on the AuNPs/SPCE electrode, new peaks were recorded at 1080, 1140, 1189, and 1395 cm^{-1}, which correspond to the polymer membrane of the *p*-ATP monomers. These peaks represent the vibration of the C−S group, the stretching of the C−H bond, and the combination of the C−H bond stretching and the C−C group vibration, respectively.[30] The Raman peaks at 480, 840, 1420, and 1653 cm^{-1} are characteristic of the NOR molecule. The first peak of 480 cm^{-1} represents the combination of the C−C binding vibration and the C−N group vibration. The second peak of 840 cm^{-1} defines the symmetric vibration of the C−F group. The vibration of the O−C−O group and the deformation of the methylene group were recognized by the third peak of 1420 cm^{-1}. The last peak of 1653 cm^{-1} identifies the strong vibration of the C═O group and the stretching vibration of the NH_2 group due to the influence of the piperazinyl group.[31] The Raman spectrum thus provides additional proof that NOR molecules were success-

https://doi.org/10.1021/acsomega.2c04414
ACS Omega 2023, 8, 2887−2896

Table 1. Sensitivity and Linearity of the Fabricated Sensors for NOR Measurement in two Concentration Ranges of 0.32−3.19 and 3.19−31.91 ng/mL

	0−3.19(ng/mL)		3.19−31.13(ng/mL)	
sensor	sensitivity ($\Omega/(\mu g\ mL^{-1})$)	R^2	sensitivity ($\Omega/(\mu g\ mL^{-1})$)	R^2
NOR-MIP/AuNPs/SPCE	326.88	0.95	37.13.	0.96
$HAuCl_4$-NOR-MIP/AuNPs/SPCE	1011.57	0.97	78.49	0.95
AuNPs-NOR-MIP/AuNPs−SPCE	631.69	0.99	112.11	0.99

Table 2. Comparison of Different Techniques for NOR Detection

technique	materials	LoD ($\mu g\ mL^{-1}$)	detection range ($\mu g\ mL^{-1}$)	references
electrochemical analysis	carbon nanotubes	0.016	0.032−31.913	34
ultraviolet (UV) spectrophotometry	hydrochloride acid	0.67	2.0−7.0	35
visible (VIS) spectrophotometry	hydrochloride acid	22.05	90−120	35
electrochemical analysis	glassy carbon electrode	1.1	5−50	36
electrochemical analysis	pyrrole	0.015	0.032−2.553	20
HPLC	sodium starch glycolate	2.185	5−20	37
electrochemical analysis	poly (amidoamine) dendrimer-encapsulated au	0.00038	0.001−10	12
electrochemical analysis	AuNPs-pATP	0.00015	0.00015−0.03113	this study

fully imprinted into the MIP film. This is further confirmed by the fact that there were no specific peaks of NOR antibiotics in the Raman spectrum upon template removal.

To confirm the recombination of artificial receptors with NOR molecules, we analyzed the Raman spectrum of the MIP-covered electrode upon exposure to a NOR solution. The resulting spectrum shows the aforementioned specific peaks of NOR molecules with a lower intensity than that of the MIP membrane. This result indicates that NOR molecules recombined with their artificial receptors (specific imprinters). The lower intensity of the peaks can be explained by the fact that some of the binding cavities did not re-bind any NOR molecules. Additionally, these peaks are absent in the Raman spectrum of the NIP-covered electrodes. This indicates that the peaks of NOR molecules on the MIP sensor originated entirely from the recombination between the NOR molecules and the compensative cavities.

3.2. EIS Spectra of the Fabricated Sensors toward NOR. *3.2.1. Performance of NOR-MIP/AuNPs/SPCE and NIP/AuNPs/SPCE.* To assess the rebinding capacity of the sensor, the MIP-covered electrodes were exposed to an increasing concentration of NOR ranging from 0.32 to 31.91 ng/mL. The resulting EIS spectra were recorded and are summarized in Figure 3a,b (NOR-MIP/AuNPs/SPCE and NIP/AuNPs/SPCE, respectively). The results show that the diameter of the semicircle in a Nyquist plot of EIS (corresponding to the R_{CT} value) increases as the NOR concentration increases for the MIP-covered SPCE. The increase in R_{CT} can be explained by the recombination of the NOR molecule with the imprinted cavities on the surface of the electrode, which decreases electron transport through the electrode. Based on eq 1, the sensitivity of the sensor is calculated at 66.32 Ω/ppb.[32]

$$S = \frac{\Delta R_{CT}(\Omega)}{\text{concentration(ng/mL)}} \quad (1)$$

This effect on the other hand is absent for the NIP-covered electrodes, where the R_{CT} of NIP/SPCE increased insignificantly when the concentration of NOR increased (Figure 3b). In particular, the NOR concentration rises from 0.32 (1 nM) to 31.91 ng/mL (100 nM), while the R_{CT} only changes by 0.1 kΩ (compared to 2.0 kΩ for NOR-MIP/SPCE). Because NOR-MIP/SPCE has no imprinted cavities on the surface, there is no re-binding between NOR and the imprinted cavities. The results indicated that the signal of NOR-MIP/SPCE was due to the re-bonding of NOR molecules with their imprinted bio-receptors on the surface of the electrode.

3.3. Performance of $HAuCl_4$-NOR-MIP/AuNPs/SPCE and AuNPs-NOR-MIP/AuNPs/SPCE. It is undeniable that the sensitivity of the NOR-MIP/AuNPs/SPCE sensor is relatively limited. In an attempt to increase the responsiveness of the sensor to NOR, the layers were doped with AuNPs as previously mentioned. The resulting EIS spectra in Figure 3c,d show the EIS spectra of the doped MIP-covered sensors, when exposing them to NOR in a concentration that increases from 0.32 to 31.91 ng/mL. The sensitivity values of $HAuCl_4$-NOR-MIP/AuNPs/SPCE and AuNPs-NOR-MIP/AuNPs/SPCE are 183.67 and 183.67 Ω/ppb, respectively. Figure 3e represents the calibration plot of the independence of ΔR_{CT} (calculated by the value of R_{CT} of the sensor at a certain NOR concentration compared to the blank sample) on NOR concentration. As shown in Figure 3e, the dose−response curve displays two linear regions: (i) in the low NOR concentration regime from 0.32 to 3.19 ng/mL and (ii) at higher NOR concentrations are from 3.19 to 31.91 ng/mL. The values also illustrate that doping the electrodes with AuNPs results in a more pronounced concentration-dependent increase in ΔR_{CT}, further proving that the sensor with the AuNPs-doped MIP membrane has a higher sensitivity than the sensor without doped AuNPs.

The sensitivity of the signal to the NOR concentration was calculated for each type of electrode and is summarized in Table 1 to examine the effect of doping in more detail. These data show that the sensitivity of NOR-MIP/AuNPs/SPCE is the lowest. In addition, its linearity, R^2 = 0.95 in the low concentration region and R^2 = 0.96 in the higher concentration region is also lower. $HAuCl_4$-NOR-MIP/AuNPs/SPCE showed the highest sensitivity in the low concentration region (0.32−3.19 ng/mL). However, the sensitivity in the high concentration region was lower than that of AuNPs-NOR-MIP/AuNPs/SPCE. Although AuNPs-NOR-MIP/AuNPs/SPCE had lower sensitivity in the low concentration region, it had higher linearity in both concentration regions (R^2 = 0.99).

https://doi.org/10.1021/acsomega.2c04414
ACS Omega 2023, 8, 2887−2896

Based on these measurements, AuNPs-NOR-MIP/AuNPs–SPCE were selected for detecting NOR concentrations in real samples. Although the sensitivity in the low concentration region of this sensor is not as high as that of $HAuCl_4$-NOR-MIP/AuNPs/SPCE, this sensor has higher sensitivity in the high concentration region and a high degree of linearity.

In order to compare the sensitivity of the sensor to that of other platforms in literature, the LoD was calculated for the optimal configuration using the 3-sigma method via the following equation

$$\mathrm{LOD} = \frac{3 \cdot \mathrm{STDEV(blank)}}{\mathrm{slope}} \quad (2)$$

In which STDEV (blank) is the average error value of the R_{CT} of the blank and the Slope is the sensitivity calculated in Table 1.[33] Based on the equation, the LoD of the AuNPs-NOR-MIP/AuNPs/SPCE sensor is 0.15 ng/mL. In comparison with many different techniques applied for NOR detection, the fabricated sensor has a lower detection limit as well as a wider linear concentration range as can be seen from the comparative analysis outlined in Table 2.

3.4. Selectivity of the Fabricated NOR Sensor. Selectivity is one of the most crucial factors in evaluating the quality of sensors in order to avoid false-negative results. In this study, we examined the selectivity of the sensor in complex samples containing other interfering antibiotics, namely, chloramphenicol (CAP), ciprofloxacin (CF), and levofloxacin (LEVO). We examined the sensor response at concentrations of 3.19 ppb (10 nM), 12.76 ppb (40 nM), and 19.14 ppb (60 nM). Figure 4a presents the response in the R_{CT} value of the NOR-MIP sensor when exposed to pure solutions containing these compounds. At a concentration of 12.76 ppb, the R_{CT} values of CAP, CF, LEVO, and NOR were 0.58, 0.50, 0.51, and 4.56 kΩ, respectively. This shows that the sensor only shows a limited response to the analogues despite the high degree of structural similarity to the target. This illustrates that the sensor performs excellently in terms of selectivity.

To further assess the selectivity of the AuNPs-NOR-MIP/AuNPs/SPCE sensor, we investigated the behavior of the sensor in complex mixtures containing both NOR and other antibiotics at the same concentration of 3.19 ppb (10 nM), 12.76 ppb (40 nM), and 19.14 ppb (60 nM) (Figure 4b). At a concentration of 19.14 ppb, the AuNPs-NOR-MIP/AuNPs/SPCE sensor measuring NOR-only, NOR-mixed CAP, NOR-mixed CF, and NOR-mixed LEVP had R_{CT} values of 4.59, 4.48, 4.48, 4.87, and 4.76 kΩ, respectively. The results clearly show that there is only a minor difference between the signal of the mixed solutions and the solution containing only NOR. This further confirms that the sensor is highly selective.

3.5. Performance in Real Samples. The determination of the concentration of antibiotics in pharmaceuticals is one of the most important applications to which attention should be paid. The fabricated AuNPs-NOR-MIP/AuNPs/SPCE sensor was applied to determine the NOR concentration in a pharmaceutical sample. After treatment, the drug sample was diluted to a concentration of 1 ng/mL and analyzed for the electrochemical signal.

Then, we measured the blank sample and obtained the charge transfer resistance value R_{CT} of 0.60 kΩ. Next, 2 μL of the diluted drug solution (1 ng/mL) was dripped onto the surface of the electrode. The change in the charge transfer resistance value compared with the blank ΔR_{CT} is 0.80 kΩ.

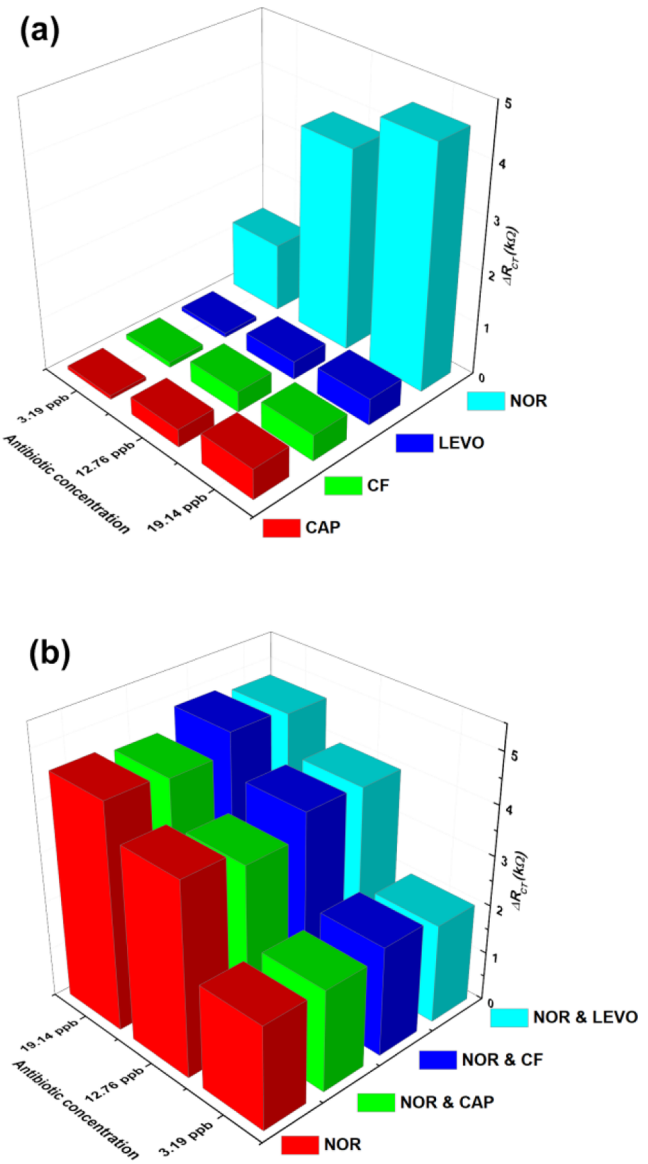

Figure 4. Response of the NOR-MIP/EIS sensor exposed to (a) pure solutions containing each antibiotic and (b) complex mixtures containing both NOR and another antibiotic.

Afterward, 2 μL of different concentrations (3, 10, and 30 ng/mL) of the diluted drug was dripped onto the electrode and analyzed electrochemically. The results show that the value of charge transfer resistance increased compared to the blank sample (Figure 5a). Three sensors were measured in this way to demonstrate reproducibility. The results show that the R_{CT} value changes very little (~5%). The results were compared with the standard curve of the sensor to determine the amount of antibiotics in the drug (shown in Table 3). Calculating the initial value before dilution and the average value of four antibiotic concentrations after dilution, we calculated the value of antibiotic concentration as 398.03 ± 0.53 mg. This value deviates by 0.5% compared to the value provided by the manufacturer (400 mg), which is acceptable in the pharmaceutical industry.

To demonstrate the performance of the sensor in real-life applications such as the detection of antibiotics in aquaculture or environmental samples, water samples from a fishpond at a local aquaculture farm were selected for antibiotic residue

https://doi.org/10.1021/acsomega.2c04414
ACS Omega 2023, 8, 2887−2896

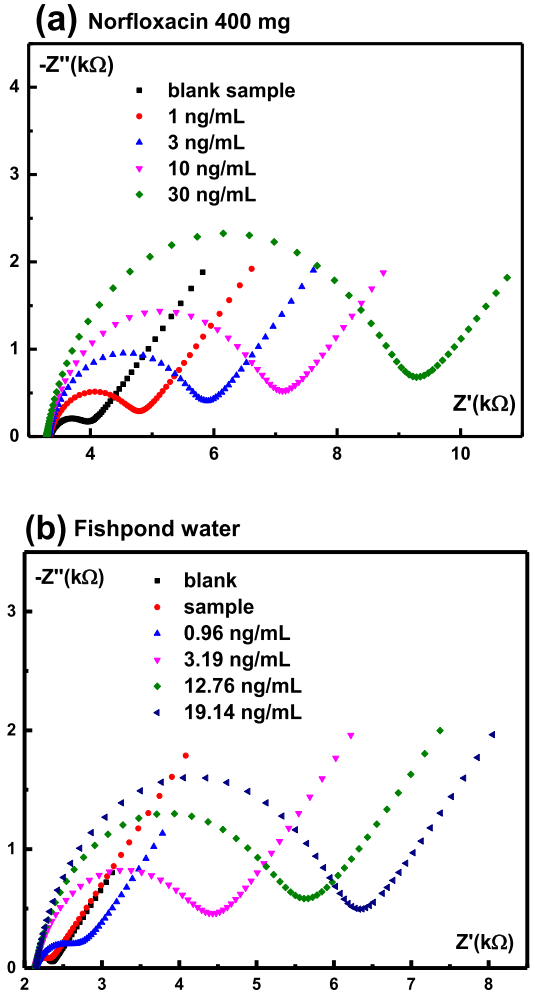

Figure 5. EIS spectrum of the NOR-MIP/EIS sensor toward (a) drug sample (NOR 400 mg) diluted to a concentration of 1, 3, 10, and 30 ng/mL and (b) fishpond water before and after adding 0.96, 3.19, 12.76, and 19.14 ng/mL of NOR.

Table 3. Concentration of Antibiotic NOR after Dilution was Determined by Electrochemical Analysis

antibiotic concentration after dilution (ng/mL)	ΔR_{CT} (Ω)	detected antibiotic concentration (ng/mL)	RSD (%)
1	676.7 (±33.8)	1.07 (±0.05)	7.00
3	1796.7 (±89.8)	2.90 (±0.14)	3.34
10	2983.7 (±149.2)	9.65 (±0.51)	3.50
30	5172.7(±258.6)	29.36 (±1.43)	2.20

analysis. After being treated and refrigerated, the water from this fishpond was analyzed by electrochemical analysis via the AuNPs-NOR-MIP/AuNPs/SPCE sensor. The charge transfer resistance value, or R_{CT}, of the blank sample measured, was 0.20 kΩ. Then, 2 μL of treated aquarium water was dripped onto the sensor for 15 min and washed twice with DI water. Next, EIS was applied to detect NOR, and the R_{CT} value measured was 0.22 kΩ. To verify the result, we analyzed two other water samples prepared with the same treatment process. The results show that the charge transfer resistance values change very little (<0.05 kΩ). This shows that the sensor accurately detects that little to no antibiotics were present in the native samples. To verify if the sensor would also reliably quantify the presence of antibiotics in this type of water sample, the pond water samples were spiked with antibiotics and the analysis was repeated. The samples were spiked with four concentrations of 0.96, 3.19, 12.76, and 19.14 ng/mL. Figure 5b shows the electrochemical characteristic curve of the sensor after analyzing the water sample added with NOR antibiotics. The results showed that the charge transfer resistance values increased when standard antibiotics were added to the aquarium water. This proves that under the actual conditions of having many different antibiotics and complex biological components, NOR molecules can still recombine with their compensative cavities. The charge transfer resistance values for three measurements displayed that the intersample variability is very low (<5%) (Table 4).

Table 4. Results of Real Sample Analysis (Water in Fishpond)

added concentration (ng/mL)	found concentration (ng/mL)	recovery (%)
0.96	0.94	98.68
3.19	3.23	101.43
12.76	12.02	94.17
19.14	18.75	97.91

4. CONCLUSIONS

The results presented in this study show that it is possible to electrochemically synthesize a MIP on screen-printed carbon electrodes and use it for antibiotic detection in real samples. In particular, the sensor based on AuNPs-NOR-MIP/AuNPs–SPCE is evaluated to be potential for NOR measurement thanks to its high sensitivity, good selectivity, and LoD. Doping the receptor layers with AuNPs improves the sensitivity by at least a factor of 2, resulting in an impedimetric sensor that has an ultralow detection limit and a wide linear range. The sensor was benchmarked using a commercial narcotic compound and is able to detect its template in relevant concentrations with little to no intersample variability or cross-selectivity observed. Taking its easy production process and potential for miniaturizing into account, these results show that the presented sensor has a large application potential in environmental and agricultural screening.

AUTHOR INFORMATION

Corresponding Author

Lien Thi Ngoc Truong − *Vietnam-Korea Institute of Science and Technology, Hanoi 100000, Vietnam; School of Engineering Physics, Hanoi University of Science and Technology, Hanoi 100000, Vietnam*; Phone: +84-912-640-015; Email: truongtnlien@gmail.com, ttnlien@most.gov.vn

Authors

Oanh Thi Vu − *Vietnam-Korea Institute of Science and Technology, Hanoi 100000, Vietnam*

Quoc Hao Nguyen − *Department of Chemical Engineering (Integrated Engineering), Kyung Hee University, Yongin-si, Gyeonggi-do 17104, Republic of Korea*

Tin Nguy Phan − *Vietnam-Korea Institute of Science and Technology, Hanoi 100000, Vietnam*; orcid.org/0000-0002-3294-9822

https://doi.org/10.1021/acsomega.2c04414
ACS Omega 2023, 8, 2887−2896

Thanh ThuyThi Luong − *National Institute of Occupational and Environmental Health, Hanoi 3800 016, Vietnam*
Kasper Eersels − *Sensor Engineering Department, Faculty of Science and Engineering, Maastricht University, Maastricht 6200 MD, The Netherlands;* orcid.org/0000-0002-0214-1320
Patrick Wagner − *Department of Physics and Astronomy, Laboratory for Soft Matter and Biophysics, KU Leuven, Leuven B-3001, Belgium;* orcid.org/0000-0002-4028-3629

Complete contact information is available at: https://pubs.acs.org/10.1021/acsomega.2c04414

Notes

The authors declare no competing financial interest.

■ ACKNOWLEDGMENTS

The author would like to thank the receipt of a grant from Vietnam National Foundation for Science and Technology Development (NAFOSTED), contract number 103.99-2017.333.

■ REFERENCES

(1) Van Giau, V.; An, S. S. A.; Hulme, J. Recent Advances in the Treatment of Pathogenic Infections Using Antibiotics and Nano-Drug Delivery Vehicles. *Drug Des., Dev. Ther.* **2019**, *13*, 327−343.
(2) Agrawal, B.; Chandra, P.; Goyal, R. N.; Shim, Y. B. Detection of Norfloxacin and Monitoring Its Effect on Caffeine Catabolism in Urine Samples. *Biosens. Bioelectron.* **2013**, *47*, 307−312.
(3) Shen, L. L. Molecular Mechanisms of DNA Gyrase Inhibition by Quinolone Antibacterials. *Adv. Pharmacol.* **1994**, *29*, 285−304.
(4) Scholar, E.*Norfloxacin. xPharm: The Comprehensive Pharmacology Reference*; Elsevier, 2007; Vol. *1*.
(5) Liu, C.; Feng, X.; Qian, H.; Fang, G.; Wang, S. Determination of Norfloxacin in Food by Capillary Electrophoresis Immunoassay with Laser-Induced Fluorescence Detector. *Food Anal. Methods* **2015**, *8*, 596−603.
(6) Rosa, T. M.; Roveda, A. C.; da Silva Godinho, W. P.; Martins, C. A.; Oliveira, P. R.; Trindade, M. A. G. Electrochemical Cell Designed for in Situ Integrate Microextraction and Electroanalysis: Trace-Level Determination of Norfloxacin in Aqueous Samples. *Talanta* **2019**, *196*, 39−46.
(7) Sher, M.; Hussain, M. A.; Mehmood, M. H.; Hassan, M. N.; Bashir, S. Bioequivalence of Norfloxacin by HPLC-UV Method. *J. Chil. Chem. Soc.* **2010**, *55*, 203−205.
(8) da Silva, A. C. A.; Matias, E. F. F.; Rocha, J. E.; de Araújo, A. C. J.; de Freitas, T. S.; Campina, F. F.; Costa, M. S.; Silva, L. E.; do Amaral, W.; Maia, B. H. L. N. S.; Ferriani, A. P.; Bezerra, C. F.; Iriti, M.; Coutinho, H. D. M. Gas Chromatography Coupled to Mass Spectrometry (GC-MS) Characterization and Evaluation of Antibacterial Bioactivities of the Essential Oils from Piper Arboreum Aubl., Piper Aduncum L. e Piper Gaudichaudianum Kunth. *Zeitschrift für Naturforschung C* **2021**, *76*, 35−42.
(9) Lapthorn, C.; Dines, T. J.; Chowdhry, B. Z.; Perkins, G. L.; Pullen, F. S. Can Ion Mobility Mass Spectrometry and Density Functional Theory Help Elucidate Protonation Sites in "small" Molecules? *Rapid Commun. Mass Spectrom.* **2013**, *27*, 2399−2410.
(10) Teng, P.; Gao, D.; Yang, X.; Luo, M.; Kong, D.; Gao, S.; Liu, Z.; Li, Z.; Wen, X.; Yuan, L.; Li, K.; Bowkett, M.; Copner, N. In Situ SERS Detection of Quinolone Antibiotic Residues in a Water Environment Based on Optofluidic In-Fiber Integrated Ag Nanoparticles. *Appl. Opt.* **2021**, *60*, 6659−6664.
(11) Yuan, Y.; Li, B.; Bin, L. Preliminary Study of Qualitative and Quantitative Detection of Norfloxacin Based on Terahertz Spectroscopy. *Int. J. Agric. Biol. Eng.* **2017**, *10*, 262−268.
(12) Liu, B.; Li, M.; Zhao, Y.; Pan, M.; Gu, Y.; Sheng, W.; Fang, G.; Wang, S. A Sensitive Electrochemical Immunosensor Based on PAMAM Dendrimer-Encapsulated Au for Detection of Norfloxacin in Animal-Derived Foods. *Sensors* **2018**, *18*, 1946.
(13) Ye, C.; Chen, X.; Zhang, D.; Xu, J.; Xi, H.; Wu, T.; Deng, D.; Xiong, C.; Zhang, J.; Huang, G. Study on the Properties and Reaction Mechanism of Polypyrrole@norfloxacin Molecularly Imprinted Electrochemical Sensor Based on Three-Dimensional CoFe-MOFs/AuNPs. *Electrochim. Acta* **2021**, *379*, 138174.
(14) Yarman, A.; Kurbanoglu, S.; Jetzschmann, K. J.; Ozkan, S. A.; Wollenberger, U.; Scheller, F. W. Electrochemical MIP-Sensors for Drugs. *Curr. Med. Chem.* **2018**, *25*, 4007−4019.
(15) Ertürk, G.; Mattiasson, B. Molecular Imprinting Techniques Used for the Preparation of Biosensors. Sensors. *Sensors* **2017**, *17*, 288.
(16) Kadhem, A. J.; Gentile, G. J.; de Cortalezzi, M. M. F. Molecularly Imprinted Polymers (Mips) in Sensors for Environmental and Biomedical Applications: A Review. *Molecules* **2021**, *26*, 6233.
(17) El-Schich, Z.; Zhang, Y.; Feith, M.; Beyer, S.; Sternbæk, L.; Ohlsson, L.; Stollenwerk, M.; Wingren, A. G. Molecularly Imprinted Polymers in Biological Applications. *BioTechniques* **2020**, *69*, 406−419.
(18) Baker, Z. K.; Sardari, S. Molecularly Imprinted Polymer (MIP) Applications in Natural Product Studies Based on Medicinal Plant and Secondary Metabolite Analysis. *Iran. Biomed. J.* **2021**, *25*, 68−77.
(19) Adumitrăchioaie, A.; Tertiş, M.; Cernat, A.; Săndulescu, R.; Cristea, C. Electrochemical Methods Based on Molecularly Imprinted Polymers for Drug Detection. *Int. J. Electrochem. Sci.* **2018**, *1*, 2556−2576.
(20) da Silva, H.; Pacheco, J.; Silva, J.; Viswanathan, S.; Delerue-Matos, C. Molecularly Imprinted Sensor for Voltammetric Detection of Norfloxacin. *Sens. Actuators, B* **2015**, *219*, 301−307.
(21) Haghdoust, S.; Arshad, U.; Mujahid, A.; Schranzhofer, L.; Lieberzeit, P. A. Development of a MIP-Based QCM Sensor for Selective Detection of Penicillins in Aqueous Media. *Chemosensors* **2021**, *9*, 362.
(22) Ayankojo, A. G.; Reut, J.; Ciocan, V.; Öpik, A.; Syritski, V. Molecularly Imprinted Polymer-Based Sensor for Electrochemical Detection of Erythromycin. *Talanta* **2020**, *209*, 120502.
(23) Diouf, A.; Bouchikhi, B.; El Bari, N. A Nonenzymatic Electrochemical Glucose Sensor Based on Molecularly Imprinted Polymer and Its Application in Measuring Saliva Glucose. *Mater. Sci. Eng. C.* **2019**, *98*, 1196−1209.
(24) Phi Van, T.; Nguy, T. P.; Truong, L. T. N. A Highly Sensitive Impedimetric Sensor Based on a MIP Biomimetic for the Detection of Enrofloxacin. *Anal. Methods* **2022**, *14*, 2195−2203.
(25) Truong, T. N. L.; van Toan, P.; Hao, N. Q. Using AuNPs-Modified Screen-Printed Electrode in the Development of Molecularly Imprinted Polymer for Artificial Bioreceptor Fabrication to Improve Biosensor Sensitivity for 17/I-Estradiol Detection. *Adv. Nat. Sci.: Nanosci. Nanotechnol.* **2019**, *10*, 015015.
(26) Do, T. T. N.; Van Phi, T.; Nguy, T. P.; Wagner, P.; Eersels, K.; Vestergaard, M. C.; Truong, L. T. N. Anisotropic In Situ-Coated AuNPs on Screen-Printed Carbon Surface for Enhanced Prostate-Specific Antigen Impedimetric Aptasensor. *J. Electron. Mater.* **2017**, *46*, 3542−3552.
(27) Nguy, T. P.; Van Phi, T.; Tram, D. T. N.; Eersels, K.; Wagner, P.; Lien, T. T. N. Development of an Impedimetric Sensor for the Label-Free Detection of the Amino Acid Sarcosine with Molecularly Imprinted Polymer Receptors. *Sens. Actuators, B* **2017**, *246*, 461−470.
(28) Li, J.-G.; Tsai, C.-Y.; Kuo, S.-W. Fabrication and Characterization of Inorganic Silver and Palladium Nanostructures within Hexagonal Cylindrical Channels of Mesoporous Carbon. *Polymers* **2014**, *6*, 1794−1809.
(29) Mariotti, D.; Švrček, V.; Mathur, A.; Dickinson, C.; Matsubara, K.; Kondo, M. Carbon Nanotube Growth Activated by Quantum-Confined Silicon Nanocrystals. *J. Phys. D: Appl. Phys.* **2013**, *46*, 122001.

(30) Osawa, M.; Matsuda, N.; Yoshii, K.; Uchida, I. Charge Transfer Resonance Raman Process in Surface-Enhanced Raman Scattering from p-Aminothiophenol Adsorbed on Silver: Herzberg-Teller Contribution. *J. Phys. Chem.* **1994**, *98*, 12702−12707.
(31) Sahoo, S.; Chakraborti, C. K.; Behera, P. K.; Mishra, S. C. FTIR and Raman Spectroscopic Investigations of a Norfloxacin/Carbopol934 Polymerie Suspension. *J. Young Pharm.* **2012**, *4*, 138−145.
(32) McGrath, M. J.; Scanaill, C. N.Sensing and Sensor Fundamentals. *Sensor Technologies*; Apress, 2013; pp 15−50.
(33) Virgilio, A.; Silva, A. B. S.; Nogueira, A. R. A.; Nóbrega, J. A.; Donati, G. L. Calculating Limits of Detection and Defining Working Ranges for Multi-Signal Calibration Methods. *J. Anal. At. Spectrom.* **2020**, *35*, 1614−1620.
(34) Huang, K. J.; Liu, X.; Xie, W. Z.; Yuan, H. X. Electrochemical Behavior and Voltammetric Determination of Norfloxacin at Glassy Carbon Electrode Modified with Multi Walled Carbon Nanotubes/Nafion. *Colloids Surf., B* **2008**, *64*, 269−274.
(35) Chierentin, L.; Salgado, H. R. N. Performance Characteristics of UV and Visible Spectrophotometry Methods for Quantitative Determination of Norfloxacin in Tablets. *J. Sci. Res.* **2014**, *6*, 531−541.
(36) Ghoneim, M. M.; Radi, A.; Beltagi, A. M. Determination of Norfloxacin by Square-Wave Adsorptive Voltammetry on a Glassy Carbon Electrode. *J. Pharm. Biomed. Anal.* **2001**, *25*, 205−210.
(37) Córdoba-Borrego, M.; Córdoba-Díaz, M.; Córdoba-Díaz, D. Validation of a High-Performance Liquid Chromatographic Method for the Determination of Norfloxacin and Its Application to Stability Studies (Photo-Stability Study of Norfloxacin). *J. Pharm. Biomed. Anal.* **1999**, *18*, 919−926.

NOTE ADDED AFTER ASAP PUBLICATION

This paper published online on January 9, 2023, with errors in Table 1. The corrected version reposted January 10, 2023.

https://doi.org/10.1021/acsomega.2c04414
ACS Omega 2023, 8, 2887−2896